Table 2. *Information on the powder data set and refinement*

For all single-crystal techniques all 527 structure factors were used.

Measurement parameters	
Radiation	Cu $K\alpha_1$, λ = 1.5405 Å
Observation range	$6.0 \le 2\theta \le 92.0°$
Step width	0.01°
Measurement time per step	3 s
Repetition factor	20
Total measurement time	6 days
No. of expected lines	527
resolved	321
overlapping	206
overlapping groups	95
Rietveld results	
No. of parameters	79
Unweighted R value	18.15
Weighted R value	15.11
R_{Bragg}	9.88

single-crystal work ($R = 0.012$; Bram, Brüderl, Burzlaff, Karayannis, Lange & Spengler, 1994) is in good agreement with the assumed conformation of the molecule, so these data are used as a reference. A comparison of the different results shows that the deviations from the correct model after refinement are of the same order as those deviations occurring directly after the structure determination. The average and maximal deviations (*cf.* Table 1, last line) give a weak indication that the application of single-crystal refinement techniques after an adequate profile-fitting procedure might lead to better results. It is supposed that the main reason for the poor behaviour is systematic errors in the intensity measurement process and that must be investigated more carefully. On the other hand the example shows that the powder data technique can be successfully applied to crystal structure determination even in the case of a medium-sized organometallic compound.

The authors would like to thank the Internationales Büro des Forschungszentrums Jülich and the GSRT in Athens for support.

References

*ATARI CRYSTAN*88 (1989). In *Proceedings of the CIC Meeting*. Berlin: Springer Verlag.
BISH, D. L. & HOWARD, S. A. (1988). *J. Appl. Cryst.* **21**, 86–91.
BRAM, A., BRÜDERL, G., BURZLAFF, H., KARAYANNIS, M I., LANGE, J. & SPENGLER, R. (1994). *Acta Cryst.* In the press.
BRÜDERL, G., BURZLAFF, H. & PERDIKATSIS, B. (1994). *J. Appl. Cryst.* In the press.
JANSEN, J., PESCHAR, R. & SCHENK, H. (1992). *J. Appl. Cryst.* **25**, 231–236.
PRESS, W. H., FLANNERY, B. P., TEUKOLSKY, S. A. & VETTERLING, W. T. (1992). In *Numerical Recipes*. New York: Cambridge Univ. Press.
RIETVELD, H. M. (1969). *J. Appl. Cryst.* **2**, 65–71.
Siemens (1993). *DIFFRAC/AT*. Siemens, Socabim.
VISSER, J. W. (1969). *J. Appl. Cryst.* **2**, 89–95.

Acta Cryst. (1994). B**50**, 50–59

Description of Coordination Geometry in Tetrahedral Metal Complexes by Symmetry-Deformation Coordinates

BY GERHARD KLEBE* AND FRANK WEBER

Main-Laboratory of BASF-AG, Carl-Bosch-Strasse, D-67056 Ludwigshafen/Rh., Germany

(*Received* 19 *January* 1993; *accepted* 6 *September* 1993)

Abstract

Coordination geometries of transition-metal complexes with Co, Ni, Cu, Pt, Pd and Rh have been analyzed by means of symmetry-deformation coordinates. These allow classification of the crystallographically observed coordination geometries with respect to reference structures of higher symmetry. Four-coordinate transition-metal complexes exhibit geometries which range from tetrahedral to square-planar. Whereas Co, Ni and Cu are found in tetrahedral, planar and various intermediate geometries, Pt, Pd and Rh mainly adopt planar coordination. Deformations retaining planarity show distortions from square to rectangular geometry. Complexes formed with monodentate ligands are less distorted than those containing chelate ligands. A preference for planar coordination is observed in chelated Co, Ni and Cu complexes. The data distribution indicates two alternative interconversion pathways, for the reversible transformation of a tetrahedral into a square-planar arrangement, according to angular compression- and twist-type deformations.

* Author for correspondence.

Introduction

Symmetry coordinates are a valuable tool to describe molecular distortions, especially of fragments in molecular structures, relative to a reference structure of higher symmetry (Murray-Rust, Bürgi & Dunitz, 1979). They are symmetry-adapted linear combinations of internal coordinates (bond lengths and angles) that transform as irreducible representations of the symmetry group of the reference structure. Planoid and other distortions of quarternary carbon in strained spiro compounds have been classified in terms of symmetry coordinates of the regular tetrahedron (Luef, Keese & Bürgi, 1987; Luef & Keese, 1992).

Four-coordinated transition-metal complexes are known to occur in geometries that range from tetrahedral to square planar (Beattie, 1988). In solution, square-planar nickel complexes show dynamic ligand-exchange processes that are assumed to proceed through tetrahedral intermediates (Hayter & Humiec, 1965; Gerdau & Kramolowsky, 1982; Fackler & Masters, 1980; Boere, Montgomery, Payne & Willis, 1985). Energy barriers (ΔG) in the region of 35–45 kJ mol^{-1} have been attributed to this process by La Mar & Sherman (1969). In the solid state, Ni–phosphine complexes occur, side-by-side, in both geometries (Kilbourn & Powell, 1970; refcode: DBBZPN, Fig. 1). In the crystal structure of bis(isopropylammonium) tetrachlorocopper(II), the metal ion is found with two different coordination geometries, a square-planar and a tetrahedrally distorted configuration (Anderson & Willett, 1974; refcode: IPRACU). Structural interconversions between geometric isomers of the type described are also observed in the solid state at high pressure (Ferraro & Long, 1975).

In the present paper we analyze, by means of symmetry deformation coordinates, the geometry about Ni, Co, Cu, Rh, Pd and Pt atoms in crystal structures of their tetracoordinated metal–organic complexes. Some conclusions about possible interconversion pathways are drawn.

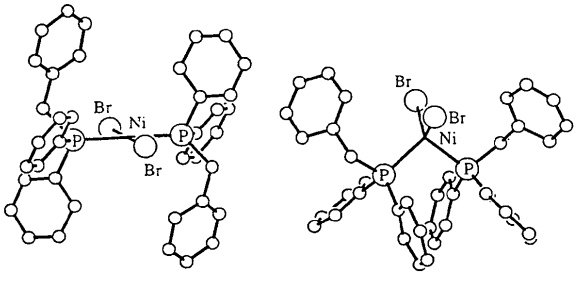

Fig. 1. Square-planar and tetrahedral coordination geometries of Ni are found side-by-side in the same crystal of dibromobis(benzyldiphenylphosphine)nickel [refcode: DBBZPN, drawing performed with the program *XP* (Sheldrick, 1988)].

Table 1. *Number of tetracoordinated metal fragments considered in each analysis, listed separately for all data (M4_all), structures with ligands bound through acyclic (M4_acyc) or cyclic bonds (M4_cyc) and bound through ligand atoms all of the same atom-type (M4_4same)*

Column 1: number of refcodes; column 2: number of independent fragments; columns 3–8: percentage of fragments that fall into areas 1–6 as defined in Fig. 6. Since these areas overlap, the total percentage may exceed 100%.

	No. of refcodes	No. of fragments	Area (in percentage) 1	2	3	4	5	6
Co4_all	279	326	52.1	16.9	13.8	4.3	6.1	0.3
Co4_acyc	173	183	78.7	2.2	2.2	2.7	2.7	0.0
Co4_cyc	97	118	5.1	46.6	39.0	4.2	9.3	3.4
Co4_4same	147	171	51.5	18.1	18.1	3.5	9.4	0.6
Ni4_all	780	786	6.4	60.1	51.5	4.8	1.1	1.1
Ni4_acyc	118	124	21.8	58.1	49.2	7.3	1.6	0.0
Ni4_cyc	563	569	1.2	63.3	59.2	3.0	0.7	1.6
Ni4_4same	425	430	3.7	61.9	64.2	3.3	0.9	1.9
Cu4_all	1474	1927	15.0	32.2	25.9	14.8	4.8	1.2
Cu4_acyc	300	338	20.7	43.8	39.3	27.5	1.2	0.0
Cu4_cyc	888	1144	3.1	36.2	33.9	9.2	4.5	4.2
Cu4_4same	587	712	6.5	40.4	38.6	19.1	3.9	4.9
Pd4_all	874	1066	0.3	62.6	36.0	0.8	0.0	0.1
Pd4_acyc	209	222	1.4	91.0	63.5	0.0	0.0	0.0
Pd4_cyc	320	409	0.0	42.5	42.3	0.5	0.0	0.2
Pd4_same	153	176	0.6	66.5	61.9	0.6	0.0	0.6
Pt4_all	1176	1401	0.5	64.2	38.9	1.7	0.1	0.3
Pt4_acyc	479	515	0.6	88.3	58.6	1.4	0.0	0.0
Pt4_cyc	220	263	0.4	37.6	55.5	0.8	0.4	0.0
Pt4_same	228	261	1.1	74.3	72.0	1.9	0.4	0.0
Rh4_all	227	312	1.6	66.3	26.3	6.4	0.3	0.3
Rh4_acyc	92	100	5.0	79.0	44.0	8.0	0.0	0.0
Rh4_cyc	29	42	0.0	33.3	11.9	11.9	0.0	2.4
Rh4_same	16	19	0.0	57.9	36.8	10.5	0.0	0.0

Data retrieval

Metal–organic complexes with central Ni, Co, Cu, Rh, Pd or Pt atoms were retrieved from the Cambridge Structural Data Base (CSD, update version July 1991; Allen *et al.*, 1979; Allen, Kennard & Taylor, 1983). In a *QUEST* search (Cambridge Crystallographic Data Center, Evaluation Program Suite), the coordination number at the metal was required to be exactly four. For each entry, internal coordinates about the metal center were calculated (*GSTAT*). In cases where a central atom occurred with two different coordination numbers in the same crystal structure, the entry was rejected from the data set. Any selection in terms of atom types (ligands bound to the metal) was achieved by the retrieval of appropriate subsets using the atom specification command in *GSTAT*. The final number of fragments used for further analysis is given in Table 1. Refcodes of the structures considered (ten pages) have been deposited as supplementary material.*

* Lists of refcodes and literature citations have been deposited with the British Library Document Supply Centre as Supplementary Publication No. SUP 71498 (16 pp.). Copies may be obtained through The Technical Editor, International Union of Crystallography, 5 Abbey Square, Chester CH1 2HU, England.

Data evaluation

For a given distorted tetracoordinated fragment there are 24 different ways in which to assign four labels to the ligand atoms in the inner coordination sphere. Starting with the initial labeling taken from the output of the *GSTAT* program, all possible permutations were calculated. On the basis of these labelings, deformations present in these four-coordinated complexes have been expressed in terms of symmetry displacement coordinates. Taking a tetrahedron as the reference polyhedron, nine such coordinates can be defined; they are given in Table 2 (Luef *et al.*, 1987). Among these S_1 and S_3 refer to distortions of bond distances, the remaining coordinates describe angular deformations. The two coordinates S_{2a} and S_{2b} are of particular interest since they describe deformations leading from tetrahedral to planar MX_4 fragments. They span a two-dimensional subspace with $3m$ symmetry, hence there are six special positions for S_{2a} and S_{2b} (Auf der Heyde, Buda & Mislow, 1991; Buda, Auf der Heyde & Mislow, 1992). The orthogonal S_{2a} and S_{2b} axes are repeated by the threefold symmetry and each of the three alternative S_{2a} axes coincides with a mirror line. For data analysis, each entry in the data set has to be projected into the same asymmetric unit of the S_{2a}/S_{2b} subspace. This projection is achieved by selecting that pair of S_{2a}/S_{2b} for which $S_{2a} > 0$, $S_{2b} > 0$ and $(3)^{1/2}S_{2a} \leq S_{2b}$. The selected deformation vector (S_{2a},S_{2b}) can still result from four different labeling schemes. To distinguish between these, a geometric condition for S_{4a}, S_{4b}, S_{4c} was chosen, such that the sum of these components is a maximum. Deformation coordinates that are based on bond distances (S_1, S_{3a}, S_{3b}, S_{3c}) require reference values (standard bond length) to be subtracted from each observed bond length, in order to describe the observed variations for all atom types on a common base. However, this problem can be avoided if only those complexes are considered in the analysis of S_1, S_{3a}, S_{3b}, S_{3c}, for which all four metal-to-ligand bonds involve atoms of the same type.

A pictorial representation of the two degenerate angular deformation coordinates S_{2a} and S_{2b} is given in Fig. 2. S_{2a} describes the mutual opening and closing of a pair of opposite angles at the metal center (retaining a local D_{2d} symmetry), at the expense of the remaining four bond angles. This coordinate has been referred to by Luef *et al.* (1987) as 'compression'. In its limit at $S_{2a} = 103.9°$, it describes a square-planar geometry, at $S_{2a} = 0$ a tetrahedron, and for negative values, the fragment degenerates towards a linear arrangement. The second coordinate ('twist' deformation) describes a twist of the two MX_2 fragments (retaining D_2 symmetry). Along this coordinate, θ_{12} and θ_{34} remain

Table 2. *Symmetry-deformation coordinates for tetrahedral symmetry*

$S_1 = (r_1 + r_2 + r_3 + r_4)/2$	A_1
$S_{2a} = 1/(12)^{1/2}(2\theta_{12} - \theta_{13} - \theta_{14} - \theta_{23} - \theta_{24} + 2\theta_{34})$	E
$S_{2b} = 1/2(\theta_{13} - \theta_{14} - \theta_{23} + \theta_{24})$	E
$S_{3a} = (r_1 + r_2 - r_3 - r_4)/2$	T_2
$S_{3b} = (r_1 - r_2 + r_3 - r_4)/2$	T_2
$S_{3c} = (r_1 - r_2 - r_3 + r_4)/2$	T_2
$S_{4a} = (\theta_{12} - \theta_{34})/(2)^{1/2}$	T_2
$S_{4b} = (\theta_{13} - \theta_{24})/(2)^{1/2}$	T_2
$S_{4c} = (\theta_{14} - \theta_{23})/(2)^{1/2}$	T_2
$S_5 = (\theta_{12} + \theta_{13} + \theta_{14} + \theta_{23} + \theta_{24} + \theta_{34} - 6\theta_0)/(6)^{1/2}$	A_1

constant while two opposing angles open up and two others close by an equivalent amount. In its limits, the geometry becomes rectangular planar (Luef *et al.*, 1987). If all angles adopt identical values (109.5°, $S_{2a} = S_{2b} = 0$), the fragment is a tetrahedron.

In Fig. 3, the S_{2a}/S_{2b} subspace is shown. The asymmetric unit, chosen by the condition mentioned above, is indicated by a solid line. Its boundaries are the positive S_{2a}, the negative S''_{2a} axes and the borderline at $S_{2a} = 103.9°$, parallel to S_{2b}. Structures that show 'pure' compression congregate along one of the three S_{2a}, S'_{2a}, S''_{2a} axes. Starting with a tetrahedral geometry (0/0°), three different square-planar coordinations (103.9/0°, −52/90°, −52/−90°) can be achieved by moving the ligand atoms parallel to one of the coordinate axes (Fig. 2, left) into the plane spanned by the other two axes (for S_{2a}: projection along the z axis so that 1–2 and 3–4 are located *trans* to each other in the xy plane; for S'_{2a}: projection along the y axis resulting in 1–3 and 2–4 being *trans*; for S''_{2a} along the x axis with 1–4 and 2–3 *trans*). Linear arrangements (103.9/180°, 103.9/−180°, −207.8/0°) are adopted moving along the S_{2a} axes in deformation space towards negative values until all atoms coincide with one of the coordinate axes (*e.g.* S_{2a}: z axis). Structures corresponding to the twist deformation aggregate along one of the S_{2b} axes, depending whether the x, y, or z axis

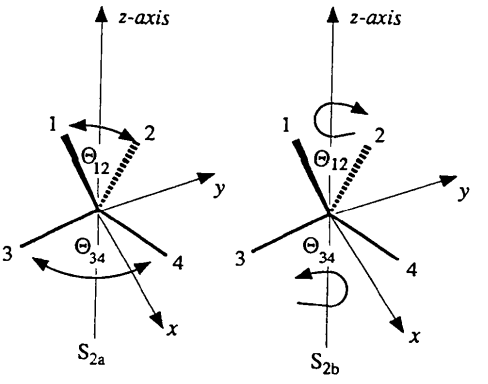

Fig. 2. Pictorial representation of the bond-angle distortions corresponding to deformations of the compression (S_{2a}, left) and twist-type (S_{2b}, right).

coincides with the direction along which the mutual twist occurs (S'_{2b}, S_{2b}, S''_{2b} axes, Fig. 2, right). Any distortion corresponding to data points located perpendicular to one of the S_{2a} axes at its upper boundary (*e.g.* 103.9/0°) describes the distortion of a square-planar into a rectangular-planar and finally into a linear fragment without changing planarity.

It is likely that in some of the structures considered in the analysis, the central metal atom coincides with a crystallographic symmetry element. In these cases, symmetry constrains the relationships among the bond angles around the central atom. The corresponding structural entries will coincide with special positions in deformation space. Accordingly, an increased population in particular areas is to be expected (*e.g.* position 0/0° in S_{2a}/S_{2b}-scatterplot for complexes with constrained tetrahedral symmetry). A detailed analysis of these symmetry-constrained structures would require a careful checking of the atomic coordinates with respect to the space group used for refinement. Considering the size of the data sets evaluated in the present study, such a detailed analysis has not been attempted.

Tetrahedral to square-planar deformations

In Fig. 4 (upper left), all tetracoordinate copper complexes (any type of ligand atom) are mapped [scattergrams were produced with the program package *SYBYL* (1991), Tripos Associates] into the part of the asymmetric unit that is indicated in Fig. 3 by the shaded area. A substantial part of this asymmetric unit, namely the region which corresponds to coordination geometries approaching a linear arrangement, is structurally not accessible because of steric repulsion of the neighboring ligands. In the remaining part of the asymmetric unit, data are not evenly distributed. Qualitatively, two main clusters are observed (areas 1 and 2, as defined in Fig. 5 with populations given in Table 1) which correspond to geometries close to tetrahedral and square-planar coordination. Apart from these two clusters, the data mainly fall close to the edges of the asymmetric unit: most of the structures align along the S_{2a}, S''_{2a} axes, which underlines the predominance of deformations of the compression type (Table 1, areas 4 and 5). Deformations of the tetrahedron towards a linear arrangement do not exceed −45° on the S''_{2a} axis. Deformations from a square-planar towards a rectangular geometry, retaining planarity, are frequently observed (Table 1, area 3); the maximum observed values of S_{2b} are listed in Table 3. These values correspond to the mean differences in bond angles between adjacent ligand atoms in the plane.

Interestingly, the central region of the structurally accessible part of the asymmetric unit is less densely

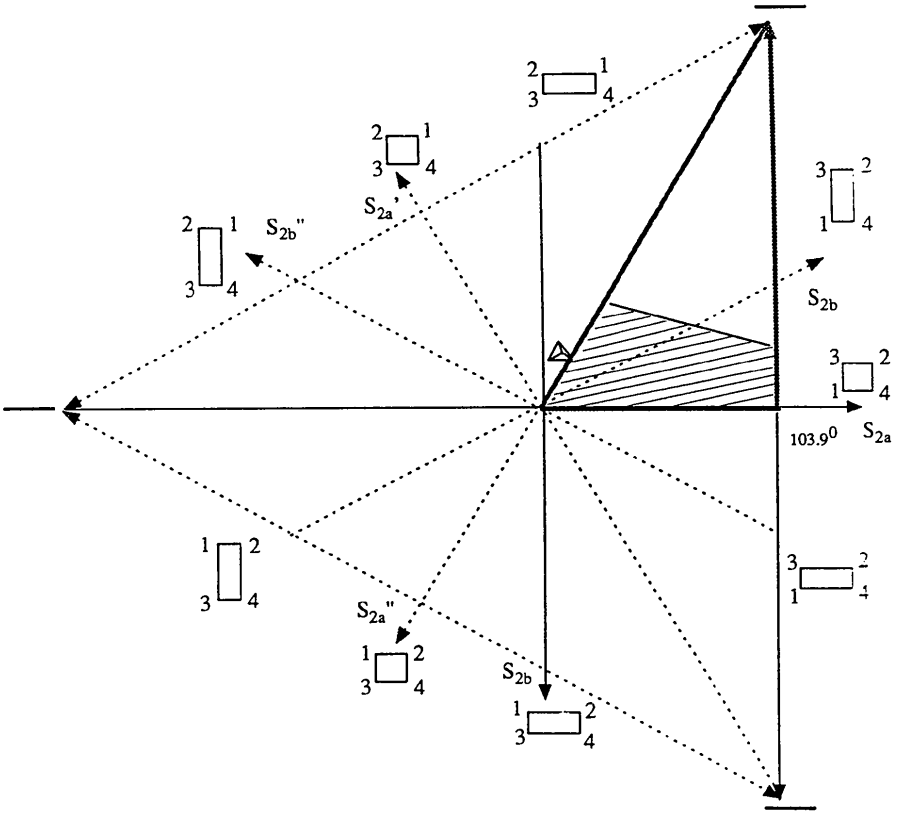

Fig. 3. Schematic representation of the S_{2a}/S_{2b} plane. Due to threefold symmetry, the S_{2a} and S_{2b} axes are repeated every 120°. At their limits, square-planar (103.9/0°, −52/90°, −52/−90°) or linear arrangements (103.9/180°, 103.9/−180°, −207.8/0°) are described, while the origin corresponds to tetrahedral coordination. Pure deformations of the compression (S_{2a}) or twist-type (S_{2b}) occur along either one of the S_{2a} or S_{2b} axes. Distortions perpendicular to one of the S_{2a} axes at the upper boundary correspond to transitions from square-planar geometry, through rectangular and towards linear geometry, while retaining planarity. The asymmetric unit is outlined by a solid line and the subspace where structural data are found has been shaded.

and rather uniformly occupied, thus no preference for a particular geometry is indicated in this part. Perhaps a slightly higher population in the region (area 6) close to the borderline towards the sterically unfavorable linear coordination geometry is evident. Pure twist-type deformations, starting with a tetrahedral geometry, should aggregate along the positive S'_{2b} axis which bisects the angle formed by the positive S_{2a} and negative S''_{2a} axes (*cf.* Fig. 3). However, as apparent from the data scatter in Fig. 4, no particular clustering of structures along this axis is indicated. The slightly more populated region (area 6) along the borderline towards the sterically unfavorable geometries, connecting maximally compressed structures with rectangular-planar arrangements, gives some evidence for the occurrence of a twist-type deformation in four-coordination geometry. Along this line (which is nearly perpendicular to S''_{2a}) an 'elongated' tetrahedron is planarized according to a twist deformation similar to that sketched in Fig. 2.

A comparison of the S_{2a}/S_{2b} maps for Cu, Ni and Co reveals similar patterns for all three metals (Fig. 4, left). Two main clusters are observed. Whereas for Ni and Cu the square-planar geometry is more frequently found, Co is seen to adopt mainly tetrahedral geometry (Table 1). For Cu, the region between square-planar and tetrahedral geometry is continuously populated, while for Ni and Co substantially fewer structures are found in this region (Table 1, area 4). Deformations along the negative S''_{2a} axis beyond a tetrahedron and towards a linear arrangement are populated in all three cases (Table 1, area 5). The same is found for the square-planar to rectangular-planar transition (area 3), except that Cu shows appreciably larger deformations than the other two metals. If the bonds formed with the metal are classified as 'cyclic' (chelate ligands) or 'acyclic' (monodentate ligands), some differences become apparent (Fig. 4, right and middle): (i) for all metals, in general, the structures with monodentate ligands show less distortions from the two higher symmetrical reference polyhedra; (ii) with chelate ligands a preference for planar coordination is observed (Table 1, areas 1 and 2); (iii) Co exhibits hardly any square-planar coordination with acyclic bound ligands, while equivalent Cu complexes span the tetrahedral to square-planar spectrum along the

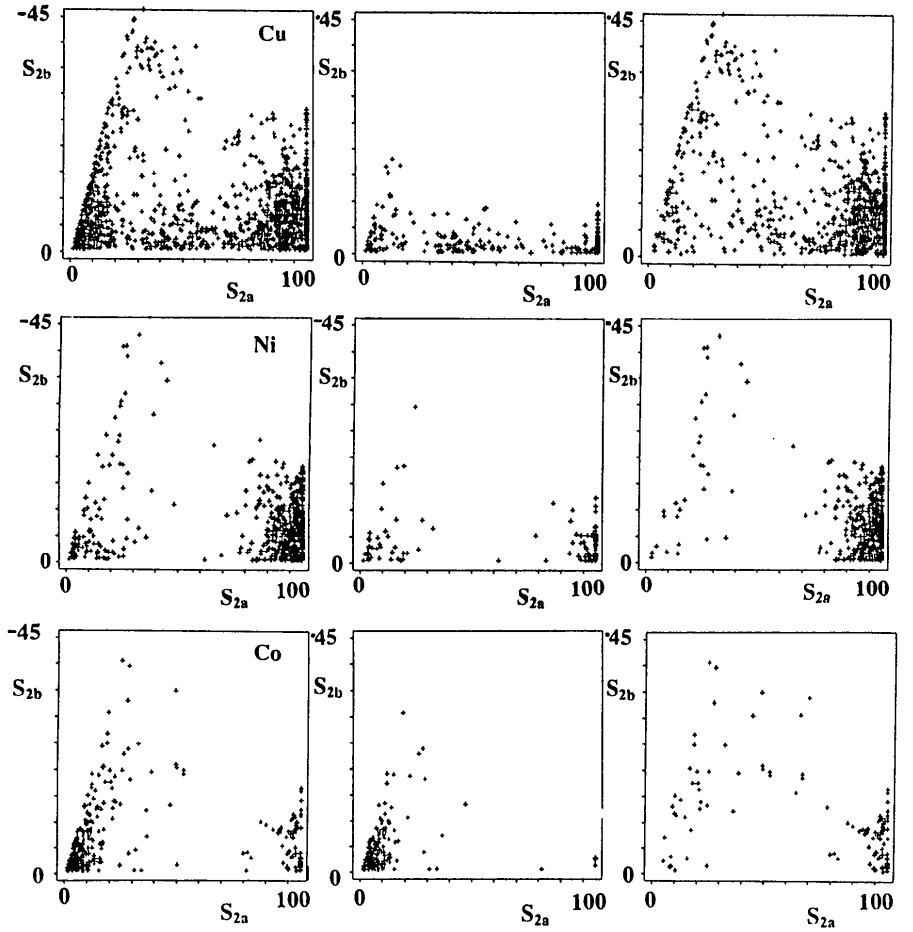

Fig. 4. Scattergrams of S_{2a} against S_{2b} (shaded area in Fig. 3): top row, Cu complexes; middle row, Ni complexes; bottom row, Co complexes; left column, all complexes; middle column, complexes with monodentate ligands (bound through acyclic bonds); right column, complexes with chelate ligands (bound through cyclic bonds; scaling of the two axes is different, thus angle between S_{2a} and $S_{2b} \neq 60°$ in the diagram).

Table 3. *Observed upper limits of the distortions along* S_{2b} (°) *for complexes with* S_{2a} *values close to* 103.9°

Refcodes of the corresponding structures are given; full literature citations have been deposited with the supplementary material. These distortions correspond to deformations with rectangular-planar geometry.

Metal	Acyclic	Refcode	Cyclic	Refcode
Co	2.3	CIYJEZ	16.1	GESTED
Ni	11.9	MTUNIB	17.3	BALVUF
Cu	9.1	BORHOF10	26.7	NDTCCU
Pd	14.3	CBMPDD10	35.5	CASPUH
Pt	16.9	GESFIT	39.4	GIGNEP
Rh	9.7	GABKOJ	16.9	VELJIF

positive S_{2a} axis, and Ni occurs approximately twice as frequently with square-planar than with tetrahedral geometry; (iv) among the acyclically coordinated tetrahedral species compression-type deformations towards a planar geometry are more frequently observed for Cu than for Ni and Co, which apparently prefer deformations towards linearity; (v) for Ni and Co, the observed deformations in structures with chelate ligands correspond to geometries lying along the negative S''_{2a} axis (area 5), to those lying along the square-planar to rectangular-planar transition (area 3) and to deformations along the borderline to the sterically inaccessible region (area 6). Only for Cu is the central region of the asymmetric unit appreciably occupied.

Complexes of Pt, Pd and Rh hardly show any tetrahedral geometry (Fig. 6, Table 1, area 1). A closer inspection of structures with geometries approaching a tetrahedron (refcodes: CASTUL, CPEPPT, CTAMTP, CUTHEE, DISDUE, GAVFAK10, KANWAX, KIJSIF, NTPHRH, PPTSOX, THOSPT, TPPTCO10, TPSOPT, TTPPDB; full literature citations have been deposited with the supplementary material) reveal formal oxidation states different from the most frequently occurring II (Pt, Pd) and I (Rh). For these metals, the observed deformations are restricted to deviations from square-planar coordination and they are more pronounced for Pd and Pt. As for Co, Ni and Cu, the absolute deformations are greater in chelate complexes than in examples with ligands coordinated through acyclic bonds. Interestingly, Rh shows less pronounced rectangular planar distortions than Pd and Pt.

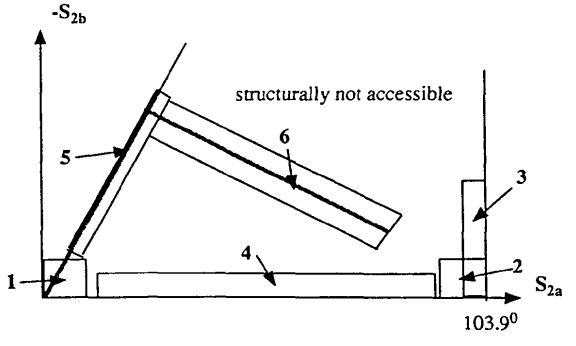

Fig. 5. Definition of different areas in the S_{2a}/S_{2b} map. Table 1 lists the percentage of the data found in these areas. Area 1: structures corresponding to tetrahedral geometry, $0° \le S_{2a} \le 10°$ and $0° \le S_{2b} \le 10°$; area 2: square-planar geometry, $93.9° \le S_{2a} \le 103.9°$ and $0° \le S_{2b} \le 10°$; area 3: transition from square- to rectangular-planar, $100° \le S_{2a} \le 103.9°$ and S_{2b} (all values); area 4: compression-type deformations between square-planar and tetrahedral geometry, $15° \le S_{2a} \le 88.9°$ and $0° \le S_{2b} \le 5°$; area 5: compression-type deformations of a tetrahedron towards linearity, $S_{2b} \ge 10°$ and $S_{2b} = (3)^{1/2} S_{2a}$, including data up to 5° from this line; area 6: data at the borderline towards the sterically inaccessible region of the asymmetric unit, data within ±5° of $S_{2b} = -1/(3)^{1/2} S_{2a} + 60°$ and $S_{2a} \le 80°$.

Bond-angle deformations along S_{4a}, S_{4b}, S_{4c}

To project all data into one single asymmetric unit of the S_{2a}/S_{2b} subspace, ligand permutations have been selected which obey the symmetry criteria (see above). For the assignments of S_{4a}, S_{4b} and S_{4c} to a particular ligand permutation, purely a geometrical criterion has been selected. Accordingly, the symmetry requirements of the $\bar{4}3m$ symmetrical S_{4a}, S_{4b}, S_{4c} subspace (Buda *et al.*, 1992) are not strictly considered and the data do not necessarily fall into one single asymmetric unit of this subspace. A scattergram of S_{4a}, S_{4b}, S_{4c} for Cu, based on such labeling, reveals a rather broad distribution; however, some clustering gives evidence for preferred distortions. Dense data scatter occurs along each of the three principle axes. This indicates that many of the complexes show distortions which correspond to deformations along one of the three coordinates: 'pure' S_{4a}, S_{4b}, S_{4c} deformations describe a simultaneous opening and closing of two opposing angles that retains C_{2v} symmetry (Fig. 7, upper row). In addition, data distribution indicates distortions which correspond to deformations described along the space diagonals: these correspond to C_{3v} symmetrical deformations that in the extreme cases yield flattened or infinitely stretched trigonal pyramids. A pictorial representation of these deformations is given in Fig. 7. For Ni and Co similar distributions are found but these are more sharply clustered along the S_{4a}, S_{4b}, S_{4c} axes. Color coding the data distribution in these scattergrams by the values for the absolute length of each deformation vector $S_2 = (S_{2a}^2 + S_{2b}^2)^{1/2}$ reveals that structures approaching a tetrahedron (S_2 small) commonly correspond to examples that are displaced from the origin in the S_{4a}, S_{4b}, S_{4c} diagram. Thus, deformations of the S_{4a}, S_{4b}, S_{4c} type are more pronounced in tetrahedral than in square-planar structures.

Equivalent scattergrams of S_{4a}, S_{4b}, S_{4c} were produced for Pt, Pd and Rh. Clustering occurs along the S_{4c}, S_{4b}, S_{4c} axes indicating preferred deformations according to one of these coordinates. Since most of

the structures in these data sets approach a planar geometry, the observed distortions correspond to bond-angle deformations similar to those sketched in Fig. 7, *i.e.* all ligand atoms in the diagrams fall close to the paper plane. As a consequence of the preference for planarity, deformations that correspond to areas close to the space diagonals in the S_{4a}, S_{4b}, S_4 space are less pronounced than for Cu, Ni, and Co.

Bond-distance deformations

To elucidate possible correlations between bond-angle and bond-distance deformations, subsets of structures composed of four ligand atoms of the same type were retrieved. For all six metals, these subsets gave S_{2a}/S_{2b} scatterplots that are similar to those obtained from all the data. Thus, non-symmetrical atom-type substitution does not appear to significantly influence coordination geometry.

A principle component analysis has been performed on these subsets for all symmetry-deformation coordinates. In all cases, the largest component can only explain about 20% of the total variance. No significant reduction in dimensionality is indicated. Apart from those correlations involving bond-angle deformations that have already been discussed, only a slight inverse dependence of S_{2a} on S_1 seems to be present. Mapping S_{3a}, S_{3b}, S_{3c} reveals that most structures cluster along the three-coordinate axes. Color coding this distribution with the 'breathing' coordinate S_1 reveals no clear-cut correlation, except perhaps a slight trend for structures to simultaneously show small S_1 and S_{3a}, S_{3b}, S_{3c} values.

Conclusions and possible interconversion pathways

Symmetry coordinates allow a classification of distortions in tetracoordinated metal complexes with respect to the higher symmetrical references, *e.g.* the tetrahedral and square-planar geometry.

Not surprisingly, Pt, Pd and Rh complexes occur mainly with planar coordination. Structures that show a strong deviation from planarity are generally associated with oxidation states that are different from the most frequently occurring states II (Pt, Pd) and I (Rh). For the first-row transition-metal complexes considered, various coordination geometries

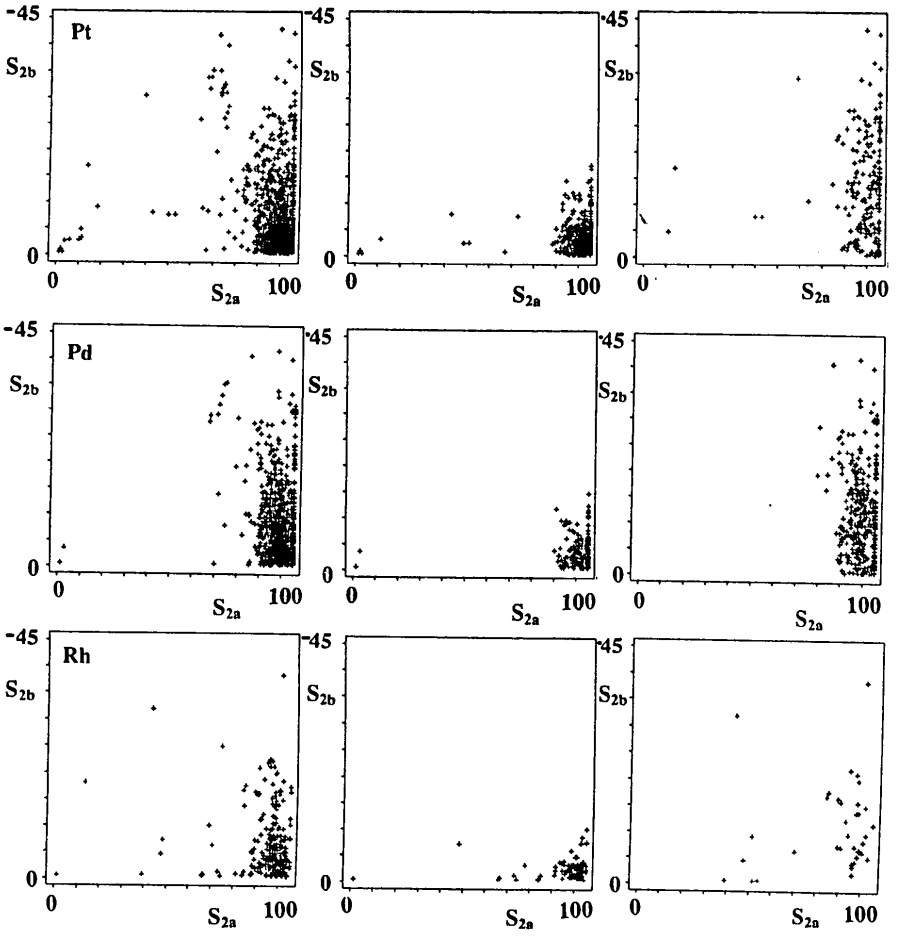

Fig. 6. Scattergrams of S_{2a} against S_{2b} (shaded area in Fig. 3): top row, Pt complexes; middle row, Pd complexes; bottom row, Rh complexes; left column, all complexes; middle column, complexes with monodentate ligands; right column, complexes with chelate ligands (scaling of the two axes is different, thus the angle between S_{2a} and $S_{2b} \neq 60°$ in the diagram).

are found. No correlation of the formal oxidation state with the coordination geometry was attempted. However, for Ni and Cu, the transition from square-planar to tetrahedral coordination occurs within the same formal oxidation state and produces changes in the electronic configuration (*cf.* absorption spectra), *i.e.* a dia- to paramagnetic transition for Ni (see *Introduction*). The weak inverse correlation of S_{2a} with S_1 may be coupled to this electronic change.

The interconversion of a square-planar into an isomeric square-planar arrangement (*e.g.* Fig. 3, labeled arrangement at 103.9/0° into that at −52/90°) *via* a tetrahedral intermediate, exchanging ligands on different sites (*e.g.* *'trans'* or *'cis'* with respect to each other), may occur without bond rupture or bond reformation. Following 'pure' compression-type deformations, *e.g.* along S_{2a} and S''_{2a}, such an exchange can be accomplished, summarized in Fig. 8. Alternatively, 'pure' twist-type deformations (*e.g.* along S'_{2b} and S''_{2b}) also allow a similar interconversion of two isometric square-planar arrangements (Fig. 9) *via* a tetrahedron. Since for both rearrangements two pairs of initially neighboring ligands remain in a short spatial relationship, complexes either formed with mono- or bidentate ligands should be capable of proceeding along these alternative pathways.

Structure correlation, established by Bürgi & Dunitz (1983), has been used to map reaction and interconversion pathways (Bürgi, 1973; Bürgi, Dunitz & Shefter, 1973; Bye, Schweizer & Dunitz, 1982; Dunitz, 1979; Britton & Dunitz, 1981; Kaftory, Nugiel, Biali & Rappoport, 1989; Nørskov-Lauritzen & Bürgi, 1985; Chandrasekar & Bürgi, 1983; Auf der Heyde & Bürgi, 1989; Klebe 1985, 1987, 1990). The method is an attempt to derive detailed structural information about a particular transformation (here square-planar to tetrahedral coordination) from a set of closely related structural fragments coming from different crystal structures (here four-coordinated metal complexes). It is assumed that the perturbations which deform the fragment under consideration (here the coordination polyhedron) are comparable with the forces which act upon a molecule along a structural transformation. The sample points of such a structure correlation tend to congregate in the low-lying regions of the potential-energy surface which underlies the pathway of the idealized fragment.

Following these ideas, two pathways can be extrapolated from the more densely populated areas of the data distribution in Fig. 4. Data along the S_{2a} axis map a pure compression pathway, interconverting tetrahedral into square planar and subsequently into an isometric tetrahedral arrangement. This path is especially indicated in the case of Cu complexes formed with monodentate ligands. A selected sample of structures which reflect snapshots along this pathway are shown in Fig. 10, the corresponding values for S_{2a} and S_{2b} are given in Table 4. Taking Cu, Ni and Co complexes formed with chelate ligands as references, some evidence is indicated for an alternative pathway involving twist-type deformations. Starting with a tetrahedral arrangement, the independent bond angles between

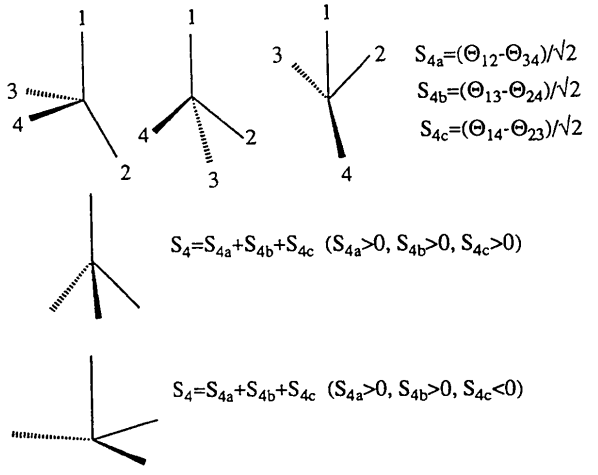

Fig. 7. Pictorial representation of the bond-angle distortions corresponding to deformations along the S_{4a}, S_{4b}, S_{4c} coordinates.

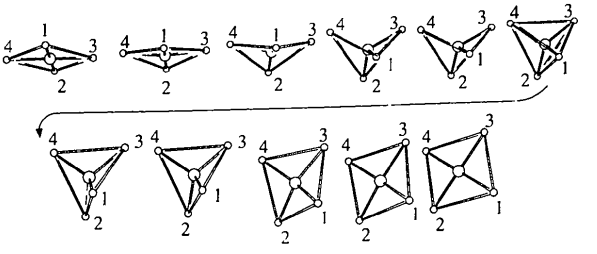

Fig. 8. Different steps along a possible isomerization pathway (*cf.* labeling) between square-planar arrangements *via* a tetrahedral intermediate. The angular changes follow 'pure' compression deformations (S_{2a}).

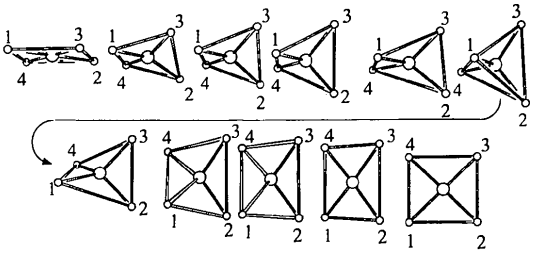

Flg. 9. Different steps along a possible isomerization pathway between square-planar arrangements *via* a tetrahedral intermediate. The angular changes follow 'pure' twist deformations (S_{2b}).

the two ligand pairs along the C_2 symmetry axis are compressed to an extremum of about 78°. Beyond this 'elongated' arrangement, a twist deformation takes place along the borderline towards the

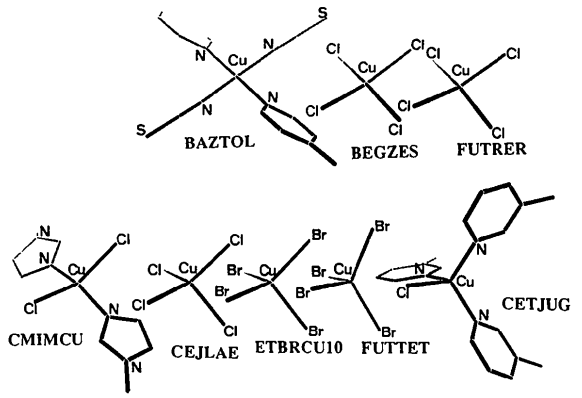

Fig. 10. Compilation of several structures (indicated by their refcodes) which resemble consecutive steps along a compression pathway from square-planar to tetrahedral geometry [BAZTOL → BEGZES → FUTRER → CMIMCU → CEJLAE → ETBRCU10 → FUTTET → CETJUG; full literature citation has been deposited with the supplementary material; drawings were produced with the program *SHADEMOL* (Hahn & Wipke, 1988)].

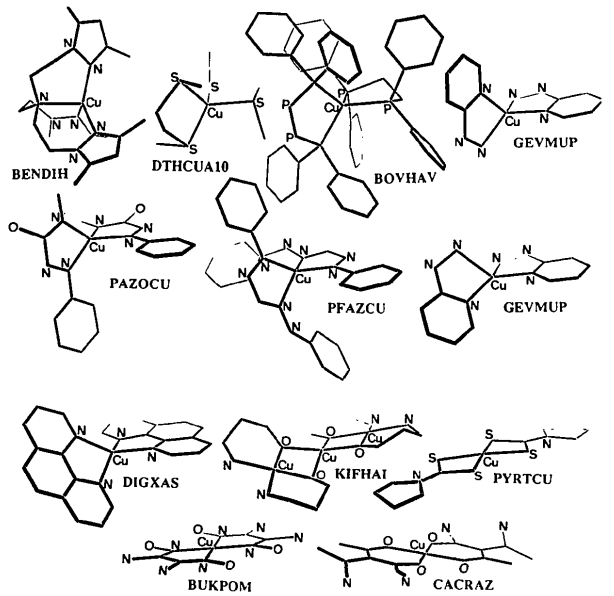

Fig. 11. Compilation of several structures (indicated by their refcodes) which resemble consecutive steps along a pathway which follows in the first part S_{2a}-type deformations of a tetrahedron towards the linear arrangement (BENDIH → DTHCUA10 → BOVHAV → GEVMUP_1), subsequently a twist deformation (PAZOCU → PFAZCU → GEVMUP_2 → DIGXAS → KIFHAI → PYRTCU), towards a rectangular-planar arrangement and finally an in-plane regularization towards a square-planar geometry (BUKPOM → CACRAZ; full literature citation has been deposited with the supplementary material).

Table 4. *Refcodes, S_{2a} and S_{2b} for several* Cu *complexes formed with ligands which are coordinated through acyclic bonds*

The complexes can be seen as a sequence of snapshots along the compression pathway from a square-planar towards a tetrahedral arrangement.

Refcode	S_{2a}	S_{2b}
BAZTOL	103.9	0.1
BEGZES	87.4	0.1
FUTRER	74.2	0.0
CMIMCU	59.9	0.5
CEJLAE	47.9	0.0
ETBRCU10	34.4	0.0
FUTTET	16.5	0.4
CETJUG	0.0	0.0

Table 5. *Refcodes, S_{2a} and S_{2b} for several* Cu *complexes formed with chelate-type ligands which can be seen as a sequence of snapshots along the transition from a tetrahedral towards a rectangular-planar arrangement*

In the first part a compression pathway towards an elongated tetrahedron is followed, which is then made planar according to a twist-type deformation.

Refcode	S_{2a}	S_{2b}
BENDIH	1.6	1.3
DTHCUA10	12.6	21.9
BOVHAV	18.8	32.4
GEVMUP	26.9	44.1
PAZOCU	31.0	45.9
PFAZCU	44.9	38.6
GEVMUP	48.1	33.9
DIGXAS	56.9	28.6
KIFHAI	79.8	25.5
PYRTCU	98.3	21.6
BUKPOM	103.9	20.3
CACRAZ	103.9	0.1

sterically inaccessible region (area 6) to result in a rectangular-planar geometry which can be regularized by in-plane bond-angle changes to a square-planar arrangement. An isometric tetrahedron is reached by proceeding along a similar pathway in reverse. Some Cu complexes which resemble situations along this pathway are compiled in Fig. 11, the corresponding values for S_{2a} and S_{2b} are given in Table 5. The suggested pathway deviates to some extent from a pure twist deformation (following one of the S_{2b} axes as indicated in Fig. 8). A compression occurs to a sterically allowed extremum, prior to a D_2 symmetrical twist deformation of two facing MX_2 fragments (Fig. 2, right). Complexes composed by two bidentate chelating groups (*cf.* Fig. 11, all examples besides BENDIH correspond to this topology) should impose structural constraints which result in favorable distortions with $S_{2a} < 0$ for tetrahedral and $S_{2b} > 0$ for square-planar geometry. Such deformations reduce steric repulsion between facing ligand atoms and allow bond angles $< 90°$ at the metal inside the chelated rings. They minimize steric hindrance along a twist-type interconversion corre-

sponding to region 6 in Fig. 6. Both pathways appear to be feasible. Supposedly, the second combined compression/twist pathway is preferentially proceeded by complexes with two chelate ligands, whereas the previous pure compression pathway is followed by complexes without steric constraints due to chelation. In addition, any preference (or combination of both) presumably depends on the electronic properties of the metal atom.

As already found in the study of spiro-carbon (Luef *et al.*, 1987), no strong correlation among bond-length deformations seems to be present.

The authors are grateful to Thomas Auf der Heyde (Bellville, South Africa) for his careful reading of the manuscript and for some important suggestions which improved this paper.

References

ALLEN, F. A., BELLARD, S., BRICE, M. D., CARTWRIGHT, B. A., DOUBLEDAY, A., HIGGS, H., HUMMELINK, T., HUMMELINK-PETERS, B. G., KENNARD, O., MOTHERWELL, W. D. S., RODGERS, J. R. & WATSON, D. G. (1979). *Acta Cryst.* B**35**, 2331–2339.

ALLEN, F. H., KENNARD, O. & TAYLOR, R. (1983). *Acc. Chem. Res.* **16**, 146–153.

ANDERSON, D. N. & WILLETT, R. D. (1974). *Inorg. Chim. Acta*, **8**, 167–175.

AUF DER HEYDE, T. P. E., BUDA, A. B. & MISLOW, K. (1991). *J. Math. Chem.* **6**, 255–265.

AUF DER HEYDE, T. P. E. & BÜRGI, H. B. (1989). *Inorg. Chem.* **28**, 3960–3989.

BEATTIE, J. K. (1988). *Adv. Inorg. Chem.* **32**, 1–53.

BOERE, R. T., MONTGOMERY, C. D., PAYNE, N. C. & WILLIS, C. J. (1985). *Inorg. Chem.* **24**, 3680–3687.

BRITTON, D. & DUNITZ, J. D. (1981). *J. Am. Chem. Soc.* **103**, 2971–2979.

BUDA, A. B., AUF DER HEYDE, T. & MISLOW, K. (1992). *Angew. Chem.* **104**, 1012–1031; *Int. Ed. Engl.* **31**, 989–1007.

BÜRGI, H. B. (1973). *Inorg. Chem.* **12**, 2321–2325.

BÜRGI, H. B. & DUNITZ, J. D. (1983). *Acc. Chem. Res.* **16**, 153–161.

BÜRGI, H. B., DUNITZ, J. D. & SHEFTER, E. (1973). *J. Am. Chem. Soc.* **95**, 5065–5067.

BYE, E., SCHWEIZER, W. B. & DUNITZ, J. D. (1982). *J. Am. Chem. Soc.* **104**, 5893–5898.

CHANDRASEKAR, K. & BÜRGI, H. B. (1983). *J. Am. Chem. Soc.* **105**, 7081–7093.

DUNITZ, J. D. (1979). *X-ray Analysis & Structure of Organic Molecules*. New York: Cornell Univ. Press.

FACKLER, J. P. JR & MASTERS, A. F. (1980). *Inorg. Chim. Acta*, **39**, 111–118.

FERRARO, J. R. & LONG, G. J. (1975). *Acc. Chem. Res.* **8**, 171–178.

GERDAU, T. & KRAMOLOWSKY, R. (1982). *Z. Naturforsch. Teil B*, **37**, 332–340.

HAHN, M. & WIPKE, W. T. (1988). *Tetrahed. Comput. Method.* **1**, 81–86.

HAYTER, R. G. & HUMIEC, F. S. (1965). *Inorg. Chem.* **4**, 1701–1706.

KILBOURN, B. T. & POWELL, H. M. (1970). *J. Chem. Soc.* pp. 1688–1693.

KLEBE, G. (1985). *J. Organomet. Chem.* **293**, 147–159.

KLEBE, G. (1987). *J. Organomet. Chem.* **332**, 35–46.

KLEBE, G. (1990). *Struct. Chem.* **1**, 597–616.

KAFTORY, M., NUGIEL, D. A., BIALI, S. E. & RAPPOPORT, Z. (1989). *J. Am. Chem. Soc.* **111**, 8181–8191.

LA MAR, G. N. & SHERMAN, E. O. (1969). *J. Am. Chem. Soc.* **92**, 2691–2699.

LUEF, W. & KEESE, R. (1992). *J. Mol. Struct. Theochem.* **257**, 353–368.

LUEF, W., KEESE, R. & BÜRGI, H. B. (1987). *Helv. Chim. Acta*, **70**, 534–542.

MURRAY-RUST, P., BÜRGI, H. B. & DUNITZ, J. D. (1979). *Acta Cryst.* A**35**, 703–714.

NØRSKOV-LAURITZEN, L. & BÜRGI, H. B. (1985). *J. Comput. Chem.* **6**, 216–228.

SHELDRICK, G. M. (1988). *XP-Plot Program*. Univ. of Göttingen, Germany.

TRIPOS ASSOCIATES (1991). *SYBYL*. Tripos Associates, St Louis, MO 63144, USA.

Acta Cryst. (1994). B**50**, 59–68

Structure of Sodium Ammonium (+)-Tartrate Tetrahydrate at 200, 151 and 120 K

BY Z. BROŻEK AND K. STADNICKA

Faculty of Chemistry, Jagiellonian University, ul. Ingardena 3, 30-060 *Kraków, Poland*

(*Received* 22 *January* 1993; *accepted* 19 *May* 1993)

Abstract

The crystal structure investigation of $NaNH_4(+)$-$C_4H_4O_6.4H_2O$, known also as NAT, SAT or ARS (ammonium Rochelle salt), was carried out in order to determine the absolute chirality and to trace possible structural changes in the paraelectric phase from room temperature down to the region close to the ferroelectric phase transition at about 110 K. The observed relative elongation of the thermal ellipsoids in the [100] direction and hydrogen-bonding reorganization near the temperature 150 K support the idea of either a long-range preparation to the ferroelectric phase transition or an additional structure reconstruction, possibly without symmetry changes, at about 150 K. Additionally, the structure